ARMY RESEARCH LABORATORY

Light Scattering from Deformed Droplets and Droplets with Inclusions:

Volume II. Theoretical Results

Gorden Videen, Wenbo Sun, Qiang Fu, David Secker, Paul Kaye, Richard Greenaway, Edwin Hirst, and David Bartley

ARL-TR-2228-II September 2000

The findings in this report are not to be construed as an official Department of the Army position unless so designated by other authorized documents.

Citation of manufacturer's or trade names does not constitute an official endorsement or approval of the use thereof.

Destroy this report when it is no longer needed. Do not return it to the originator.

Abstract

This is the second volume of a two-volume report dealing with experimental and theoretical results from the scattering of light by deformed liquid droplets and droplets with inclusions. With improved instrumentation and computer technologies available, researchers are able to employ two-dimensional angular optical scattering (TAOS) as a tool for analyzing such particle systems, and this could find application in industrial, occupational, and military aerosol measurements. In this report we present numerically calculated spatial light-scattering data from various droplet morphologies, which may be produced with a vibrating-orifice-type droplet generator. We describe characteristic features of the theoretical data and compare these to the experimental results given in volume I of this report.

Contents

Figures

1. Introduction

This is the second of a two-volume report dealing with experimental and theoretical results from the scattering of light by deformed liquid droplets and droplets with inclusions. Deformed droplets are an important consideration in industrial areas involving sprays, therapeutic aerosols, and combustion aerosols, where aerodynamic particle size is commonly measured to assess the airborne behavior of the droplets. Aerodynamic particle sizing instruments are known to produce droplet deformation during the measurement process, and this can lead to significant measurement errors [1]. Droplets with inclusions are important because they can be representative of aerosols found in hospital or battlefield environments, where biological organisms can survive for prolonged periods when contained within a protective liquid coating. The in-situ detection of these biological aerosols has attracted considerable attention recently, with laser-induced fluorescence being investigated as a means of discriminating biological from nonbiological particles [2,3]. However, since fluorescence is exhibited by many aerosol particles, discrimination based on this parameter alone has proved inefficient.

Light scattering provides an ideal means of in-situ particle characterization or identification, because it is rapid and, in many cases, nondestructive. While traditionally, light-scattering measurements were made using a single, movable detector or a limited number of fixed detectors, the advent of low-cost computer equipment and multi-pixel detectors, such as intensified charge-coupled device (ICCD) cameras, has made out-of-plane, two-dimensional angular optical scattering (TAOS) measurements more common for the study of nonspherical or nonhomogeneous particle systems of the type mentioned above [4–11].

At the same time that experimental equipment has increased in sophistication, great strides have been made on the modeling front. Although most of the credit should be given to the proliferation of fast computers, we should not overlook the modeling efforts made on irregular particles and the current algorithms developed to make the calculation of the scatter from irregular particles as simple and commonplace as the calculation of Mie scattering was a few decades ago. Modeling efforts have not only increased the efficiency of old algorithms like the discrete dipole approximation (DDA) [12–14], the finite-difference time-domain (FDTD) technique [15–17], and *T*-matrix techniques [18–21], but new theories have been developed to rapidly calculate the scattering from such commonly occurring particle systems as multiple spheres [22–28] and spheres containing eccentrically located inclusions [29–32].

In volume I of this report [33], we described methods for routinely acquiring light-scattering data from individual deformed droplets and droplets with inclusions and presented examples of the spatial scattering patterns resulting from these particle morphologies. We now go on to show how the scatter from these types of particles can readily be calculated (indeed, all the calculations performed here can be performed by programs currently in the public domain [34–36]).

2. Particle Systems

Mie theory predicts the electromagnetic fields scattered by a homogeneous sphere illuminated by a plane wave. When illuminated by a laser beam of sufficiently large spot size, the light-scattering total intensity can be described by concentric rings about the specular peak due to the particle symmetry. The spacing of the rings is determined by the sphere composition and, most importantly, size. In this section we describe a number of particle systems created by a vibrating-orifice-type droplet generator. The advantage of such generators is that millions of nearly identical particle systems can be periodically created, and hence, studied in great detail. So reproducible are these systems that it is even possible to adjust the vibrating frequency, and hence the particle size, and accurately measure the scatter as the particles pass through a resonance [37,38]. As described in volume I of this report [33], under certain measurement conditions, the droplets can be predictably distorted to become aspherical. We begin by examining the scatter from some of these distorted droplets.

2.1 Ellipsoids, Stadium Particles, and Other UFOs

When a normally spherical droplet is subject to an accelerating airflow, as is found in the sampling nozzle of aerodynamic particle sizing instruments, for example, it can be made to distort into one of a range of geometries, the simplest of which is spheroidal. Calculation of the scattering from spheroids is now commonplace. Several methods exist for doing this, but perhaps the most common is the T-matrix approach first developed by Waterman [18,19]. T-matrix techniques have many inherent advantages. Because of their efficient use of vector spherical harmonics, they are rapid and provide efficient means of calculating scattering properties when a particle system is illuminated at different scattering angles. An excellent review article of this technique was published by Mishchenko [21], who also maintains a website containing the source code to calculate the scattering from spheroids [35].

Despite the advantages of the T-matrix method, for a number of reasons, we performed the calculations in this section using the FDTD algorithm with a perfectly absorbing boundary layer [15]. First, extreme computational precision is necessary when one calculates the T-matrix of particles having large aspect ratios, some of which we wished to analyze. Second, improvements in the FDTD, including a perfectly absorbing boundary layer, are accurate to well within 1 percent at all scattering angles, except at minima, where the scattering is several orders of magnitude lower than the maxima [39]. Third, FDTD methods no longer have severe size-parameter restrictions [15]. And fourth, the FDTD algorithm was developed in-house, making it especially easy to modify to our needs. In this section we study a

number of droplets of different shapes. For comparison, the refractive index n, maximum physical extent D, and aspect ratio are identical for the particles we discuss in this section. In this way we hope to see the effects of the particle shape on the scattering and see what, if any, distinguishing features appear in the scattering patterns, which can help in the inversion procedure. In the simulations we present here, the aspect ratio is set to 2, the refractive index m = 1.4599 (corresponding to oleic acid at λ = 0.6328 μm), and the maximum physical extent is $D = 24\,\lambda/\pi = 4.83$ μm. We present some examples of the theoretical scatter from nonspherical droplets in figure 1. The particles in this figure are axisymmetric about the z-axis and are illuminated by a plane wave traveling in the positive x direction so that the forward scatter is located at the center of the graphs ($\theta = 90°$, $\phi = 0°$). The y-axis of our plots is the polar angle θ, the x-axis is the azimuthal angle ϕ, and the grey level shows the logarithm of the total intensity. Because of the droplet symmetry, the scattering intensities are symmetric about θ = 90°, and ϕ = 0°.

Figure 1a shows the scatter from an oblate spheroid illuminated end-on. Since scattering spatial frequencies are typically inversely proportional to particle dimensions, we expect to see the approximately elliptical concentric rings whose major axis is oriented with the particle's minor axis and vice versa. The dark horizontal bands in the figure are unexpected. The position of these bands is dependent on the particle size. As the particle size increases, the number of bands increases and their spacing decreases. Elliptical fringes and multiple interference bands are also displayed in experimental scattering measurements; for instance, one clear example is given in volume I of this report [33] in figure 4, for a 20-μm equivalent sphere and a flow rate of 5.0 l/min. Because the particle is relatively large, a high number of fringes can be seen in this example.

Some of the particle images demonstrated in volume I [33] suggest that under certain conditions of droplet size, viscosity, surface tension, and airflow acceleration, droplets tend to flatten out further and become "stadium particles." Stadium cylinders have recently garnered some notoriety, since scattered rays from such systems have chaotic properties [40,41]. One can mathematically produce such systems by slicing an infinite cylinder in half lengthwise, pulling the two half-cylinders apart, and filling in the gap, so that the cross section resembles a rectangle capped with two semicircles, or a stadium. For three-dimensional particles, there are multiple ways to create particles with a stadium cross section: a rod capped with two hemispheres or a finite circular disk with rounded edges (resembling a jelly donut) both have similar cross sections, so both should display similar chaotic properties. Because stadium rods and disks do not have edges or discontinuities in their spatial derivatives, they are used to simulate finite cylinders and plates in scattering calculations. The scattering from the stadium particle resembling a jelly donut is shown in figure 1b. The scattering from this system is significantly different from that of an ellipsoid. Two

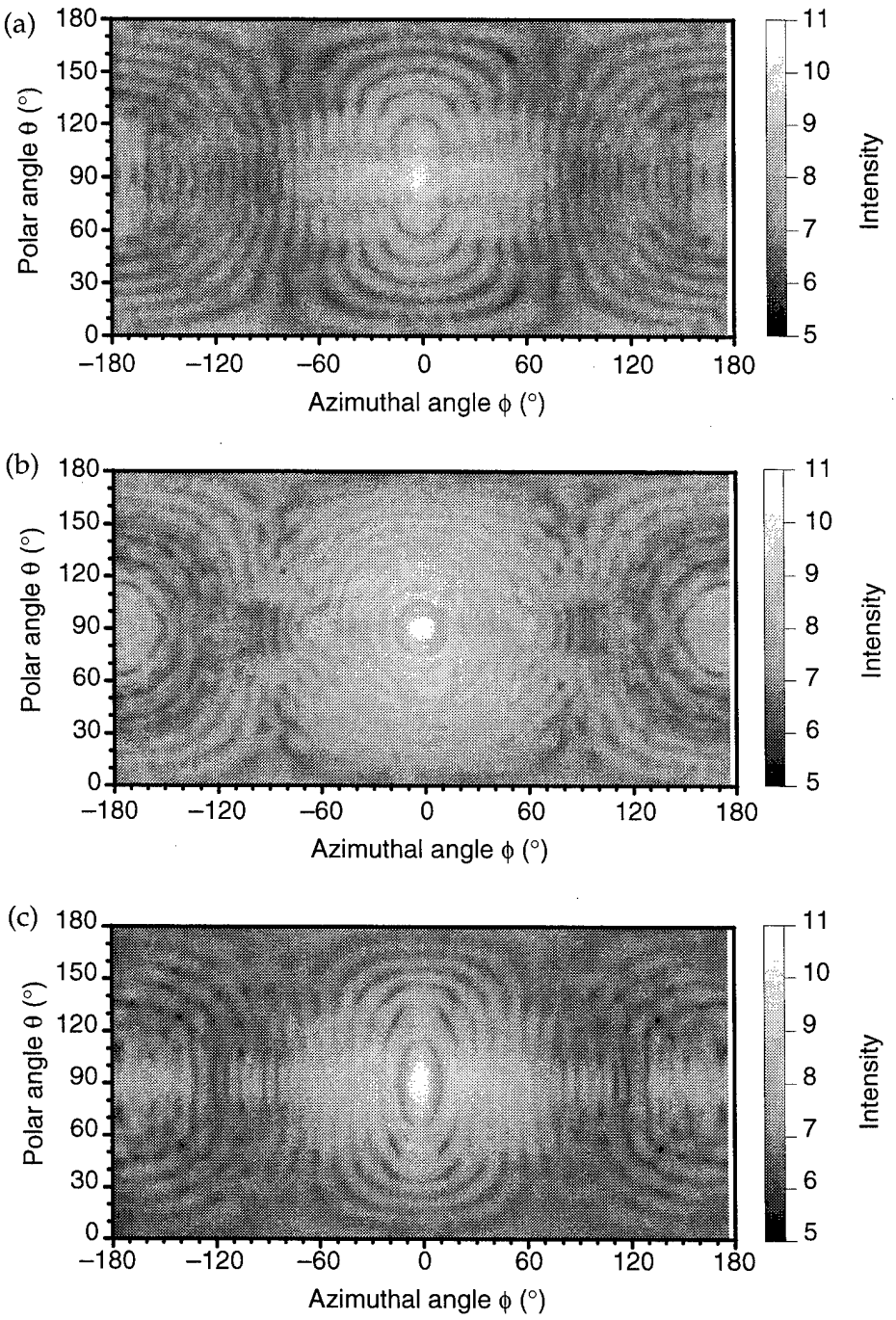

Figure 1. Two-dimensional angular optical scattering calculated from number of aspherical oleic acid (n = 1.4599) droplets illuminated edge-on at λ = 0.6328 μm. Ratio of largest to smallest dimension is set equal to 2 for all cases, and size parameter (in terms of largest particle extent D) is $x = \pi D/\lambda = 24$. Forward scattering is located at center of graphs. Droplet shapes are (a) oblate ellipsoid, (b) toroidal disk, and (c) droplet of form $r = r_o + d(1 - 3\cos^2\theta)$.

distinct sets of fringes are visible. Concentric circular fringes are the result of the spherical caps. Superimposed on this pattern are concentric ovals, elongated in the horizontal direction. The nearly flat edges of the scattering fringes are due to the edge of the disk. Interestingly, none of the experimental patterns shown in volume I [33] displayed these characteristics. We present these examples to demonstrate how sensitive the scattering is to particle shape. The particles in figures 1a and 1b have the same dimensions and vary only slightly in shape, but their scattering is significantly different.

We consider one other particle shape in this section, that of a quadrupole toroidal, again shown in volume I of this report [33]. This type of distorted droplet, similar in shape to a human erythrocyte (red blood cell), is produced in an accelerating flow field and can be calculated analytically with the Navier-Stokes equation [42]. The droplet is of the form

$$r = r_o + d(1 - 3\cos^2 q)\,, \tag{1}$$

where r_o is the radius of an undistorted droplet, and d is the amount of distortion. The droplet is axisymmetric about the z axis. For the droplet to have an aspect ratio of 2, the amount of distortion $d = 0.246\, r_o$. The scattering from this particle displays a semi-elliptic ring structure similar to that of the oblate spheroid particle shown in figure 1a, but instead of the multiple bands seen for the spheroid, this particle displays a single high-intensity streak running through the minor axis of the scatter ellipses. Faint, dark bands radiate from the center of the scattering pattern in the form of an x. This scattering pattern bears a strong resemblance to several of the experimental patterns shown in volume I (fig. 4 and 5) [33].

2.2 Satellites

Depending on the vibrating frequency and droplet size and composition, droplets ejected from the vibrating orifice may break up or come into close proximity with other droplets [43]. In such cases, the resulting scattering system resembles either two spheres of nearly identical size or one large (host) sphere with a much smaller (satellite) sphere in close proximity. It may be impossible to optically isolate the multiple droplets, and the resulting scattered light is the superposition of the scattered light from both particles. Depending on the relative proximity of the droplets, significant interaction may occur between the two subparticle systems. Many theoretical solutions to the scattering from multiple particle subsystems have been derived [10,22–28] and programmed [34]. Reaching a solution is relatively straightforward. The scattered field from every subsystem is considered to be part of the incident field on every other subsystem. One reaches the solution by performing vector translations of these scattered fields from one subsystem coordinate system onto the other subsystem coordinate systems and satisfying the boundary conditions at the interfaces of every subsystem. This process requires knowledge of how to translate vector spherical harmonics from one coordinate system to another and the T-matrix for each subsystem. For spherical particles, many symmetries exist in the T-matrix, and when only two spherical droplets are considered, additional symmetries in the translation coefficients make the calculations rapid. For the calculations in this section, we use the program developed by Videen, Ngo, and Hart [27], available at the website maintained by Thomas Wriedt [34].

In our studies we examine two spheres approximating two oleic acid droplets (m = 1.4599) illuminated at λ = 0.6328 μm. Droplets exit the vibrating orifice along the negative z-axis. Due to spatial constraints of the experimental system, they are illuminated by a laser beam whose wavevector is

perpendicular to this droplet flow. The incident wavevector is in the $\hat{x}$ direction, so the droplets are illuminated broadside. We vary the droplet radii r_1 and r_2 and separation distance d between the droplets and examine the dependence of scattering features on these parameters. Figure 2a shows the scattering from a pair of equal-radius $r_1 = r_2 = 2\lambda$ spheres, whose centers are separated by a distance $d = 5\lambda$. The forward-scatter ($\theta = 90°$, $\phi = 0°$) maximum is surrounded by concentric rings of minima and maxima, similar to what we would expect from a single Mie sphere. Because of the droplet symmetry, the scattering intensities are symmetric about $\theta = 90°$, and $\phi = 0°$. The major effect of the scattering from two spheres is the interference, which is visible in figure 2a as maxima and minima at constant θ. The minima are most apparent. These minima are due to the interference of the rays scattered by the identical droplets, and their positions depend primarily on the separation distance d. If there is no interaction between the spheres, the scattering from the spheres would be identical, except for a phase term. The intensity of the minima would be zero, and the minima positions would depend solely on the separation distance d. Because there is some interaction between the spheres, the minima are not zero. As d increases, the spacing between the minima decreases, as demonstrated in figure 2b, which shows the scattering from the pair of spheres shown in figure 2a, but separated by $d = 10\lambda$. Because the interaction decreases with distance, the intensity values of the minima are lower in figure 2b than in figure 2a. The Young's two-slit experiment is a similar system, and we would expect similar results. Ignoring interaction, we would expect maxima to be located at

$$ml = d\cos q\,, \tag{2}$$

where m is an integer, and we note that θ is the polar angle and not the angle measured from specular. Equation (2) holds quite well, even for spheres in close proximity, such as those of figure 2a.

When the spheres are not identical, the interference structure becomes distorted. Figure 2c shows the light-scattering intensities for a pair of spheres separated by the same spacing as the case of figure 2a, but with the top sphere four times smaller than the bottom sphere ($r_1 = 4r_2 = 2\lambda$). In this projection, the minima are no longer lines of constant θ. The contours of the minima now curve toward the larger particle as the magnitude of ϕ increases. As the separation distance between the particles increases (shown in fig. 2d), the spacing between the minima decreases, and the slopes of the minima also decrease. The positions of the nodes and antinodes can be approximated quite simply with the use of a ray-tracing model. Figure 3 shows a diagram of the two spheres and the rays that produce the interferogram. In this model, we assume that only the rays reflecting off the outer surfaces of the spheres contribute to the interference. Ray 1 strikes the surface of sphere 1 of radius r_1 placed a distance d below sphere 2 of radius r_2, which is struck by ray 2. Both rays are scattered to the detector placed in the far field at (θ, ϕ). The phase difference between these two rays can be written as

$$\Phi = kd\cos\theta + 2k(r_1 - r_2)\sin\frac{\theta'}{2}\,, \tag{3}$$

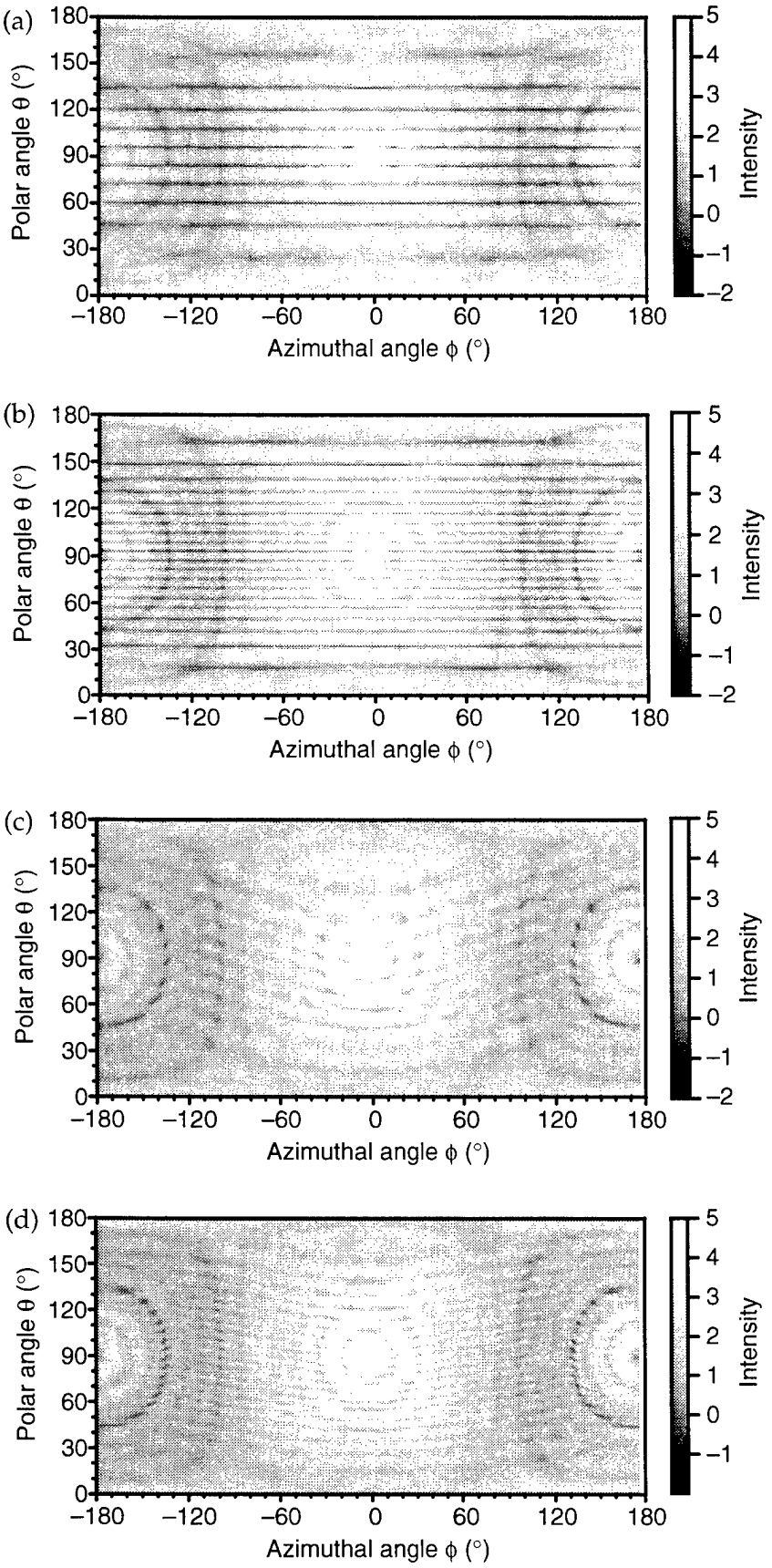

Figure 2. Two-dimensional angular optical scattering calculated from pair of spherical oleic acid (n = 1.4599) droplets illuminated at λ = 0.6328 μm. Forward scattering is located at center of graph and radii and droplet center separation distances are (a) $r_1 = r_2 = 2\lambda$, $d = 5\lambda$; (b) $r_1 = r_2 = 2\lambda$, $d = 10\lambda$; (c) $r_1 = 2\lambda$, $r_2 = \lambda/2$, $d = 5\lambda$; and (d) $r_1 = 2\lambda$, $r_2 = \lambda/2$, $d = 10\lambda$.

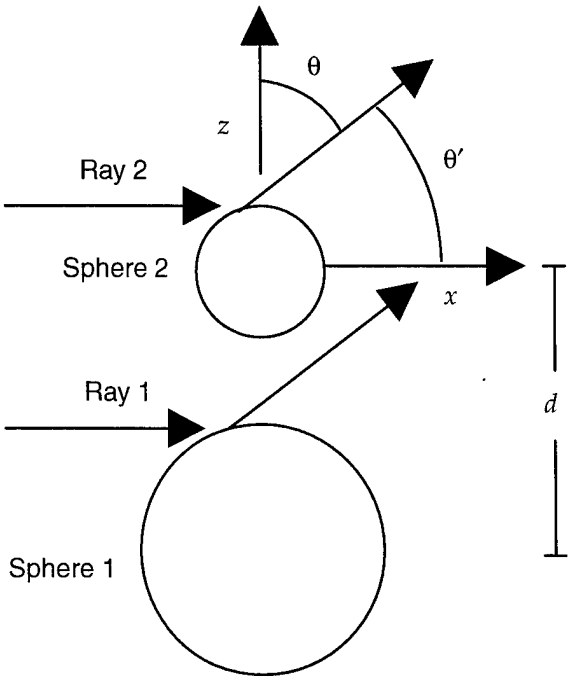

Figure 3. Configuration of model used to estimate shape of scattering maxima produced by two spheres. Sphere 1 of radius r_1 is located distance d below sphere 2 of radius r_2. Each sphere is struck by ray that is reflected off surface to detector placed in far field at (θ, ϕ). Constructive interference of these two rays can be used to predict locations of interference maxima.

where k is the wave number of the incident light, θ is the scattering angle measured from the z-axis connecting the centers of the spheres, and θ' is the scattering angle measured from the specular direction (x-axis). For the rays to interfere constructively and a maximum to appear in the scattering, the path difference between the rays must be an integer number of wavelengths. If we project the pattern onto a screen, it is convenient to express the condition for a maximum (eq (3)) as

$$m\lambda = dz/\sqrt{x^2+y^2+z^2} + (r_2 - r_1)\sqrt{2}\sqrt{1 - x/\sqrt{x^2+y^2+z^2}} \quad , \qquad (4)$$

where m is an integer. Note that if the spheres are the same size ($r_1 = r_2$), the interference is due solely to the separation distance between the spheres and the maxima trace lines of constant θ (from eq (3)), which are shown in figures 2a and 2b. On a screen placed parallel to the y-z plane, equation (4) is simplified, and these maxima are hyperbolae.

When the spheres are not the same size, the interferogram is more complicated; however, the ray-tracing solution does quite an adequate job of reproducing the maxima. Figure 4 shows the interferogram of figure 2d projected on a screen placed at x = 1 m from the centers of the spheres. Superimposed on the pattern are lines predicting the position of the maxima using equation (4). Equation (4) assumes that forward-scattered rays from each individual particle are in phase. In general, this is not the case. The result is that the predicted maxima positions are displaced. Although the predicted positions of the maxima are different from the actual positions, the contours of the maxima and the spacing between them is very accurate. This is remarkable, considering that we use a ray-tracing model and include only singly reflected rays when the sizes of the spheres are on the order of the wavelength, and refraction, interaction, and diffraction are completely

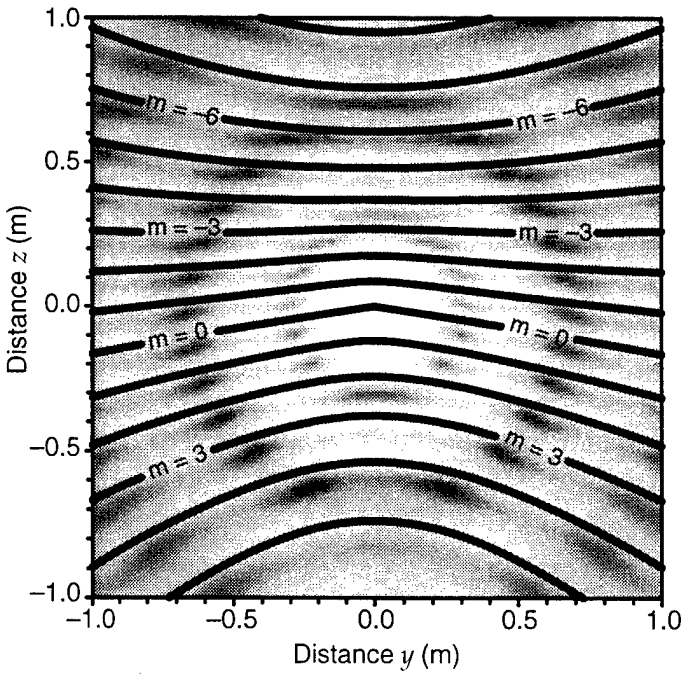

Figure 4. Scattering interferogram of pair of spherical oleic acid (n = 1.4599) droplets illuminated at λ = 0.6328 μm. Radii of droplets are $r_1 = 2\lambda$, $r_2 = \lambda/2$, and droplet center separation distance $d = 10\lambda$. Superimposed are shapes of scattering maxima predicted with equation (4).

ignored in the model. Part of the reason for the good agreement is that the change in the phase of the individual scattering amplitudes resulting from this simple model as a function of scattering angle qualitatively agrees with reality.

2.3 Inclusions

When the composition of the liquid placed in the reservoir of the vibrating-orifice droplet generator is inhomogeneous, the droplets produced by the generator may also be inhomogeneous. One type of system commonly studied is that of a liquid host containing polystyrene spheres [37,44–52]. The resonance structure and lasing properties of the host droplet have a strong dependence on the size and quantity of spherical inclusions. Such systems are easily produced, but quantifying the position and placement of the inclusions is difficult. As demonstrated in volume I of this report [33], when oleic acid droplets are created in a humid environment, it is hypothesized that water condenses onto the droplet, creating an immiscible oleic acid/water droplet. Because of the symmetry, the location of the water inclusion within the oleic acid host is centered on the z-axis. Such a system is of interest from a modeling point of view, because it contains one relatively large inclusion whose position is at least restricted to a single axis.

Many theoretical solutions to the scattering from spherical hosts containing subsystems have been derived [29–32] and programmed [34,53]. The solution is relatively straightforward. The scattered field from every subsystem within the host is considered to be part of the incident field on every other subsystem and as part of the internal fields of the host. One can reach the solution by performing vector translations of these scattered fields from

each subsystem coordinate system onto the host sphere coordinate system and satisfying the boundary conditions at all the interfaces. Like the two-sphere system, this process requires knowledge of how to translate vector spherical harmonics from one coordinate system to another and the T-matrix for every system. For spherical inclusions, many symmetries exist in the T-matrix, and when only a single spherical inclusion is considered, additional symmetries in the translation coefficients make the calculations rapid. For the calculations in this section, we use the program developed by Videen et al [32], available at the website maintained by Thomas Wriedt [34].

In our studies, we examined a spherical host oleic acid droplet ($m = 1.4599$) containing a water inclusion ($m = 1.33$) illuminated at $\lambda = 0.6328$ μm. Droplets exit the vibrating orifice along the negative z-axis. Due to spatial constraints of the experimental system, they are illuminated by a laser beam whose wavevector is perpendicular to this droplet flow (the incident wavevector is in the $\hat{x}$ direction). Because of the symmetry, we assume that the water inclusion is centered on this line of flow, the z-axis.

The most dramatic effect is the dependence of the spatial scattering on the position of the inclusion. We demonstrate this dependence in figure 5, which shows the two-dimensional angular optical scattering calculated from a spherical $r_1 = 5\lambda$ oleic acid host droplet containing a spherical $r_2 = 2.5\lambda$ water inclusion illuminated at $\lambda = 0.6328$ μm. Data from four different inclusion positions are shown. The parameter d is the distance from the center of the host droplet to the center of the inclusion. Figure 5a shows the scattering when the spheres are concentric, $d = 0$. In this case, the bright central maximum ($\theta = 90°$, $\phi = 0°$) is surrounded by concentric minima and maxima. Because of the symmetry, the scattering from the concentric sphere system is very similar to that of a homogeneous sphere. As the inclusion is moved from the center of the host particle, the symmetry is broken, and additional structure is apparent in the spatial scattering. Figure 5b shows the scattering when the inclusion is displaced one wavelength in the $\hat{z}$ direction from the host center. Although the symmetric fringe pattern seen in figure 5a remains the dominant feature, additional structure is now present. A few degrees above the central maximum (on the side opposite the inclusion), the pattern is noticeably brighter than in figure 5a, whereas a few degrees below the central maximum, the pattern is noticeably darker. Going further from the central maximum (about 30°), this is reversed, and it is darker above the central maximum and lighter below. As the inclusion is brought closer to the edge of the host (fig. 5c), a secondary ring structure becomes apparent in the scattering, centered approximately 30° above the specular peak (in the direction opposite the inclusion). In addition, two dark bands radiate outward from the specular peak, forming a V in this projection. When the inclusion is brought to the edge of the host (fig. 5d), the secondary structure changes position only slightly, but the contrast has also increased slightly. In addition, the minima nearest the specular are distorted, and they are distended on the side of the inclusion. The dominant features in figure 5

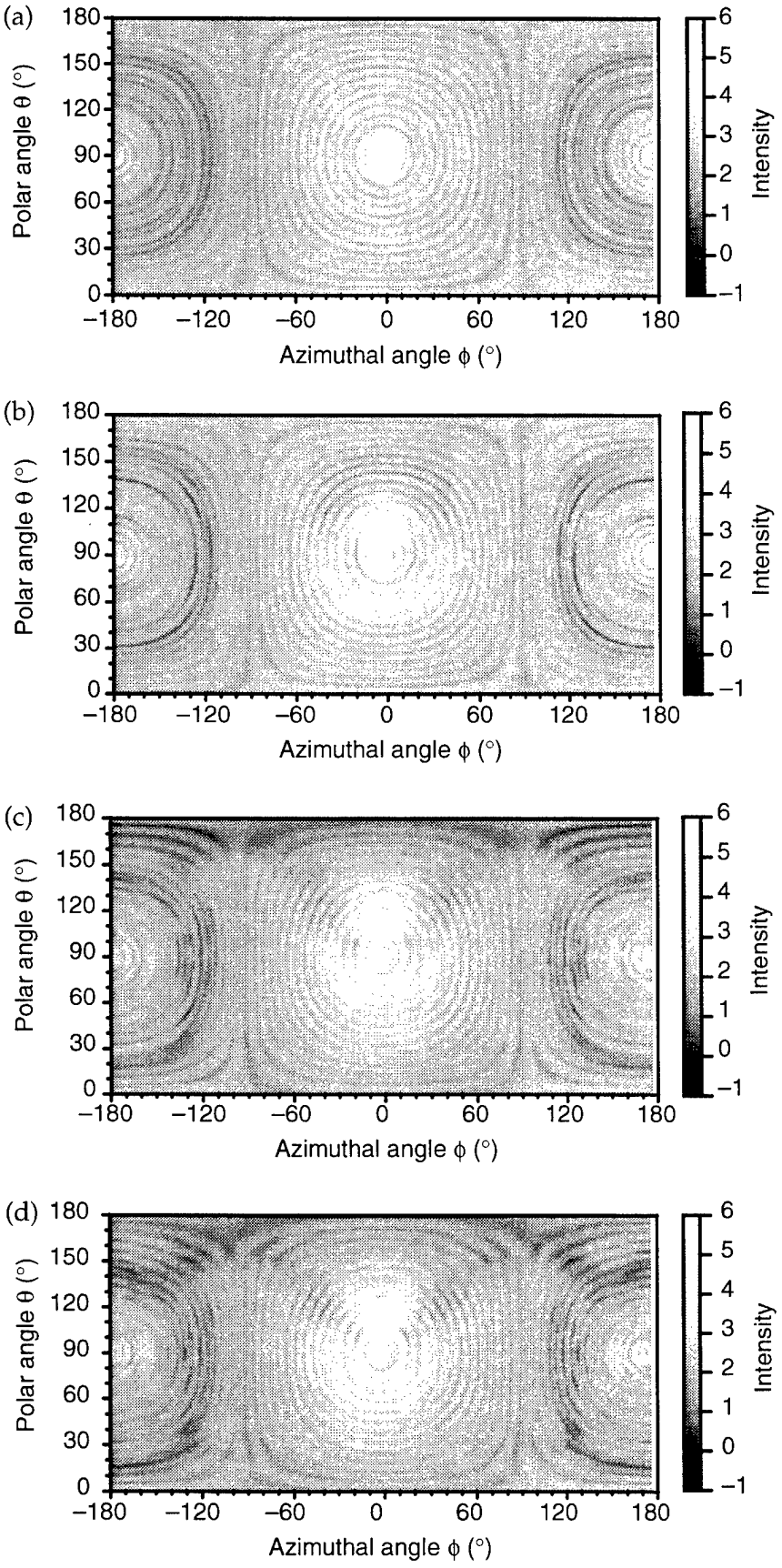

Figure 5. Two-dimensional angular optical scattering calculated from spherical $r_1 = 5\lambda$ oleic acid ($n = 1.4599$) host droplet containing spherical $r_2 = 2.5\lambda$ water ($n = 1.33$) inclusion illuminated at $\lambda = 0.6328$ μm. Distance from inclusion center to host center is (a) $d = 0\lambda$, (b) $d = 1.0\lambda$, (c) $d = 2.0\lambda$, and (d) $d = 2.4\lambda$.

are present in the experimental scattering measurements of the oleic acid host droplets containing water inclusions made by the authors and shown in volume I of this report (fig. 8 to 10) [33].

Figure 6 shows the scattering from three $r_1 = 6.0\lambda$ oleic acid host droplets containing different-size spherical water inclusions placed at the same position within the host. The scattering is projected onto a plane screen placed 1 m from the particle system. Note that the primary ring structure in this projection is now circular, and the secondary interference is below the specular (still opposite the inclusion). Figure 6a shows the scattering when the inclusion radius is $r_2 = 1.0\lambda$. Only one secondary ring is obvious for this system. As the inclusion size increases to $r_2 = 2.0\lambda$ (fig. 6b), the frequency of the secondary rings increases and so does the contrast. Further increasing the inclusion size (fig. 6c) enhances these features. In this series of scattering plots, it is apparent that the secondary ring structure is the result of host internal fields being scattered by the inclusion. Upon exiting the host droplet, these fields are refracted to the side opposite the specular peak. The frequency of this secondary ring structure is directly related to the size of the inclusion. In previous experimental work [44] cross-polarized images of host droplets containing inclusions have been described as a "ring of fireflies" that flash on and off when the inclusions enter and leave the outer (high-intensity internal field) region of the host. This observation is consistent with our simulations, which show the secondary ring structure to be more visible when the inclusions are near the outer edge of the host.

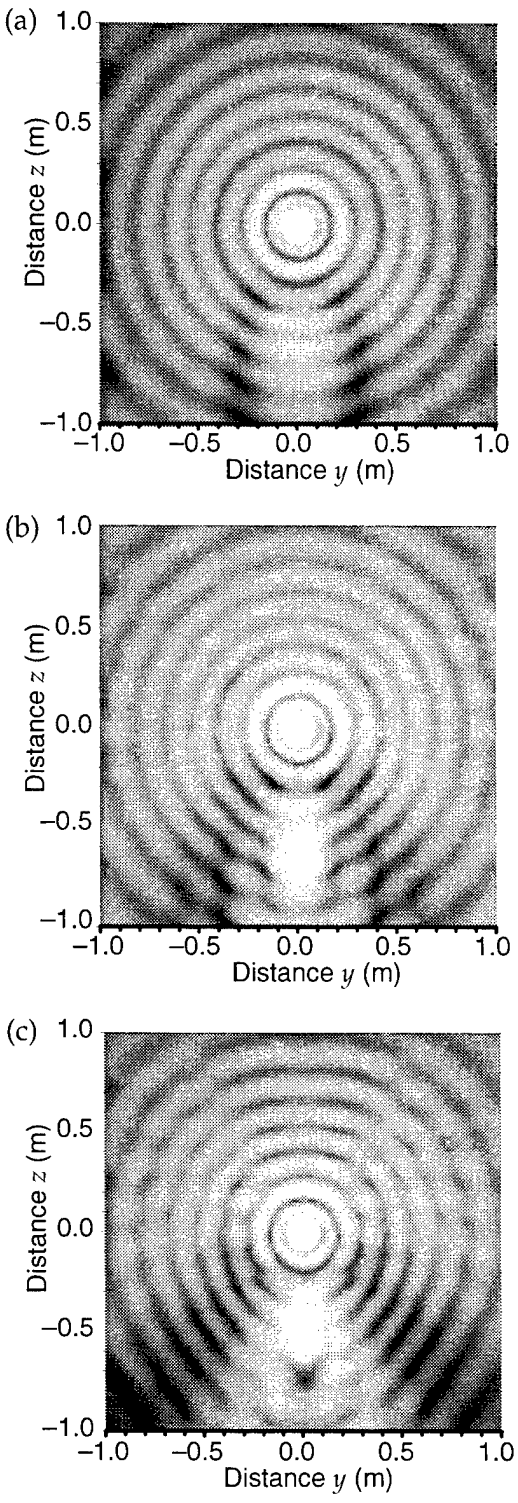

Figure 6. Two-dimensional angular optical scattering calculated from spherical $r_1 = 6\lambda$ oleic acid ($n = 1.4599$) host droplet containing spherical water ($n = 1.33$) inclusion whose center is located distance $d = 3.0\lambda$ from host center. Inclusion radius is (a) $r_2 = 1\lambda$, (b) $r_2 = 2\lambda$, and (c) $r_2 = 2.99\lambda$.

3. Conclusion

In this volume of the report, we calculate the spatial scattering from droplets with different morphologies. The theoretical scattering patterns produced here can all be replicated with the use of programs available in the public domain and, as shown in volume I of the report, can be routinely and reproducibly generated experimentally with a vibrating-orifice droplet generator and an aerodynamic focusing nozzle. Many of the features present in the light-scattering data not only identify the fundamental geometry of the particle, but can be used to quantify particle characteristics, such as the degree of deformation of droplets from their normal spherical form or the presence of inclusions within droplets. The former is important when aerodynamic particle sizing instruments are used to assess droplet behavior; the latter has importance in the field of bioaerosol detection. In the case of bisphere scattering, the interferogram produced can be reproduced quite accurately with the ray-tracing model we present in this volume of the report. After an experimental capture of an interferogram, it would be relatively trivial to perform a curve-fit to the secondary maxima to identify the particle sizes and relative positions.

Acknowledgments

This work was carried out with funding from the UK Engineering and Physical Sciences Research Council, support from TSI, Inc., St. Paul, MN, and a Department of Energy ARM Grant DE-FG02-97ER62363.

References

1. W. D. Griffiths, P. J. Iles, and N. P. Vaughan, "The behaviour of liquid droplets in an APS 3300," *J. Aerosol Sci.* **17**, 427–431 (1986).
2. R. G. Pinnick, S. C. Hill, P. Nachman, G. Videen, G. Chen, and R. K. Chang, "Aerosol fluorescence spectrum analyzer for measurement of single micron-sized airborne biological particles," *Aerosol Sci. Technol.* **28**, 95–104 (1998).
3. J. Barton, E. Hirst, P. Kaye, S. Saunders, and D. Clark, "Airborne particle characterization by spatial scattering and fluorescence," *Proc. SPIE* **3855**, 92–100 (1999).
4. A. Ashkin and J. M. Dziedzic, "Observation of light scattering from nonspherical particles using optical levitation," *Appl. Opt.* **19**, 660–668 (1980).
5. S. Holler, Y.-L. Pan, R. K. Chang, J. R. Bottiger, S. C. Hill, and D. B. Hillis, "Two-dimensional angular optical scattering for the characterization of airborne microparticles," *Opt. Lett.* **23**, 1489–1491 (1998).
6. S. Holler, M. Surbek, R. K. Chang, and Y.-L. Pan, "Two-dimensional angular optical scattering patterns as droplets evolve into clusters," *Opt. Lett.* **24**, 1185–1187 (1999).
7. M. D. Barnes, C.-Y. Kung, N. Lermer, K. Fukui, B. G. Sumpter, D. W. Noid, and J. U. Otaigbe, "Homogeneous polymer blend microparticles with a tunable refractive index," *Opt. Lett.* **24**, 121–123 (1999).
8. B. Sachweh, H. Barthel, R. Polke, H. Umhauer, and H. Buttner, "Particle shape and structure analysis from the spatial intensity pattern of scattered light using different measuring devices," *J. Aerosol Sci.* **30**, 1257–1270 (1999).
9. P. H. Kaye, K. Alexander-Buckley, E. Hirst, and S. Saunders, "A real-time monitoring system for airborne particle shape and size analysis," *J. Geophys. Res. (Atmospheres)* **101** (D14), 19,215–19,221 (1996).
10. E. Hirst and P. H. Kaye, "Experimental and theoretical light scattering profiles from spherical and non-spherical particles," *J. Geophys. Res. (Atmospheres)* **101** (D14), 19,231–19,235 (1996).
11. P. H. Kaye, "Spatial light scattering as a means of characterising and classifying non-spherical particles," *Measurement Sci. Technol.* **9** (2), 141–149 (1998).
12. B. T. Draine, "The discrete dipole approximation for light scattering by irregular targets, "*Light Scattering by Nonspherical Particles*, M. I. Mishchenko, J. W. Hovenier, and L. D. Travis, eds., Academic Press, pp 131–145 (1999).
13. B. T. Draine and P. J. Flatau, "Discrete-dipole approximation for scattering calculations," *J. Opt. Soc. Am. A* **11**, 1491–1499 (1994).

14. A. Hoekstra, J. Rahola, and P. Sloot, "Accuracy of internal fields in volume integral equation simulations of light scattering," *Appl. Opt.* **37**, 8482–8497 (1998).

15. W. Sun, Q. Fu, and Z. Chen, "Finite-difference time-domain solution of light scattering by dielectric particles with a perfectly matched layer absorbing boundary condition," *Appl. Opt.* **38**, 3141–3151 (1999).

16. P. Yang and K. N. Liou, "Finite difference time domain method for light scattering by nonspherical and inhomogeneous particles," *Light Scattering by Nonspherical Particles*, M. I. Mishchenko, J. W. Hovenier, and L. D. Travis, eds., Academic Press, pp 173–221 (1999).

17. K. S. Yee, "Numerical solution of initial boundary value problems involving Maxwell's equation in isotropic media," *IEEE Trans. Antennas Propag.* **AP-14**, 302–307 (1966).

18. P. C. Waterman, "Matrix formulation of electromagnetic scattering," *Proc. IEEE* **53**, 805–812 (1965).

19. P. C. Waterman, "Symmetry, unitarity, and geometry in electromagnetic scattering," *Phys. Rev. D* **3**, 825–812 (1971).

20. M. I. Mishchenko, "*T*-matrix method and its applications," *Light Scattering by Nonspherical Particles*, M. I. Mishchenko, J. W. Hovenier, and L. D. Travis, eds., Academic Press, pp 147–172 (1999).

21. M. I. Mishchenko, L. D. Travis, and D. W. Mackowski, "*T*-matrix computations of light scattering by nonspherical particles: A review," *J. Quant. Spectrosc. Radiat. Transfer* **55**, 535–575 (1996).

22. J. H. Bruning and Y. T. Lo, "Multiple scattering of EM waves by spheres, parts I & II," *IEEE Trans. Antennas Propag.* **AP-19**, 378–400 (1971).

23. F. Borghese, P. Denti, R. Saija, G. Toscano, and O. I. Sindoni, "Multiple electromagnetic scattering from a cluster of spheres. I. Theory," *Aerosol Sci. Technol.* **3**, 227–235 (1984).

24. D. W. Mackowski, "Calculation of total cross sections of multiple-sphere clusters," *J. Opt. Soc. Am. A* **11**, 2851–2861 (1994).

25. K. A. Fuller, "Scattering and absorption cross sections of compounded spheres. I. Theory for external aggregation," *J. Opt. Soc. Am. A* **11**, 3251–3260 (1994).

26. K. A. Fuller, "Scattering and absorption cross sections of compounded spheres. II. Calculations for external aggregation," *J. Opt. Soc. Am. A* **12**, 881–892 (1995).

27. G. Videen, D. Ngo, and M. B. Hart, "Light scattering from a pair of conducting, osculating spheres," *Opt. Commun.* **125**, 275–287 (1996).

28. K. A. Fuller and D. W. Mackowski, "Electromagnetic scattering by compounded spherical particles," *Light Scattering by Nonspherical Particles*, M. I. Mishchenko, J. W. Hovenier, and L. D. Travis, eds., Academic Press, pp 225–272 (1999).

29. J. G. Fikioris and N. K. Uzunoglu, "Scattering from an eccentrically stratified dielectric sphere," *J. Opt. Soc. Am.* **69**, 1359–1366 (1979).

30. F. Borghese, P. Denti, and R. Saija, "Optical properties of spheres containing a spherical eccentric inclusion," *J. Opt. Soc. Am. A* **9**, 1327–1335 (1992).

31. K. A. Fuller, "Scattering and absorption cross sections of compounded spheres. III. Spheres containing arbitrarily located spherical inhomogeneities," *J. Opt. Soc. Am. A* **12**, 893–904 (1995).

32. G. Videen, D. Ngo, P. Chýlek, and R. G. Pinnick, "Light scattering from a sphere with an irregular inclusion," *J. Opt. Soc. Am. A* **12**, 922–928 (1995).

33. D. R. Secker, P. H. Kaye, R. Greenaway, E. Hirst, D. Bartley, and G. Videen, *Light Scattering from Deformed Droplets and Droplets with Inclusions: Volume I. Experimental Results*. U.S. Army Research Laboratory, ARL-TR-2228-I (September 2000).

34. Website maintained by T. Wriedt: http://imperator.cip-iwl.uni-bremen.de/fg01/codes2.html.

35. Website maintained by M. I. Mishchenko: http://www.giss.nasa.gov/~crmim/.

36. Website maintained by P. J. Flatau: http://atol.ucsd.edu/~pflatau\.

37. D. Ngo and R. G. Pinnick, "Suppression of scattering resonances in inhomogeneous microdroplets," *J. Opt. Soc. Am. A* **11**, 1352–1359 (1994).

38. A. Biswas, H. Latifi, R. L. Armstrong, and R. G. Pinnick, "Time-resolved spectroscopy of laser emission from dye-doped droplet," *Opt. Lett.* **14**, 214–216 (1989).

39. G. Videen, W. Sun, and Q. Fu, "Light scattering from irregular tetrahedral aggregates," *Opt. Commun.* **156**, 5–9 (1998).

40. J. H. Jensen, "Chaotic scattering of light by a dielectric cylinder," *J. Opt. Soc. Am. A* **10**, 1204–1208 (1993).

41. J. U. Nöckel and A. D. Stone, "Ray and wave chaos in asymmetric resonant optical cavities," *Nature* **385**, 45–47 (1997).

42. D. L. Bartley, A. B. Martinez, P. A. Baron, D. R. Secker, and E. Hirst, "Droplet distortion in accelerating flow," *J. Aerosol Sci.*, in press.

43. H.-J. Moon, G.-H. Kim, Y.-S. Lim, C.-S. Go, J.-H. Lee, and J.-S. Chang, "Lasing images from two merging ink-doped liquid droplets," *Opt. Lett.* **21**, 913–915 (1996).

44. B. V. Bronk, M. J. Smith, and S. Arnold, "Photon-correlation spectroscopy for small spherical inclusions in a micrometer-sized electrodynamically levitated droplet," *Opt. Lett.* **18**, 93–95 (1993).

45. J. Gu, T. E. Ruekgauer, J.-G. Xie, and R. L. Armstrong, "Effect of particulate seeding on microdroplet angular scattering," *Opt. Lett.* **18**, 1293–1295 (1993).

46. J.-G. Xie, T. E. Ruekgauer, R. L. Armstrong, and R. G. Pinnick, "Suppression of stimulated Raman scattering from microdroplets by seeding with nanometer-sized latex particles," *Opt. Lett.* **18**, 340–342 (1993).

47. H.-B. Lin, A. L. Huston, J. D. Eversole, A. J. Campillo, and P. Chýlek, "Internal scattering effects on microdroplet resonant emission structure," *Opt. Lett.* **17**, 970–972 (1992).

48. R. L. Armstrong, J.-G. Xie, T. E. Ruekgauer, J. Gu, and R. G. Pinnick, "Effects of submicrometer-sized particles on microdroplet lasing," *Opt. Lett.* **18**, 119–121 (1993).

49. T. Kaiser, G. Roll, and G. Schweiger, "Enhancement of the Raman spectrum of optically levitated microspheres by seeded nanoparticles," *J. Opt. Soc. Am. B* **12**, 281–286 (1995).

50. G. Videen, P. Pellegrino, D. Ngo, J. S. Videen, and R. G. Pinnick, "Light-scattering intensity fluctuations in microdroplets containing inclusions," *Appl. Opt.* **36**, 6115–6118 (1997).

51. G. Videen, P. Pellegrino, D. Ngo, P. Nachman, and R. G. Pinnick, "Qualitative light-scattering angular correlations of conglomerate particles," *Appl. Opt.* **36**, 3532–3537 (1997).

52. P. Pellegrino, G. Videen, and R. G. Pinnick, "Quantitative light-scattering angular correlations of conglomerate particles," *Appl. Opt.* **36**, 7672–7677 (1997).

53. D. Ngo, G. Videen, and P. Chýlek, "A FORTRAN code for the scattering of EM waves by a sphere with a nonconcentric spherical inclusion," *Comp. Phys. Commun.* **1077**, 94–112 (1996).

Distribution

Admnstr
Defns Techl Info Ctr
Attn DTIC-OCP
8725 John J Kingman Rd Ste 0944
FT Belvoir VA 22060-6218

DARPA
Attn S Welby
Attn Techl Lib
3701 N Fairfax Dr
Arlington VA 22203-1714

Dir of Defns Rsrch & Engrg
Attn DD TWP
Attn Engrg
The Pentagon
Washington DC 20301

Ofc of the Secy of Defns
Attn ODDRE (R&AT)
The Pentagon
Washington DC 20301-3080

Ofc of the Secy of Defns
Attn OUSD(A&T)/ODDR&E(R) R J Trew
3080 Defense Pentagon
Washington DC 20301-7100

Commanding Officer
Attn NMCB23
6205 Stuart Rd Ste 101
FT Belvoir VA 22060-5275

AMCOM MRDEC
Attn AMSMI-RD W C McCorkle
Redstone Arsenal AL 35898-5240

Dir for MANPRINT
Ofc of the Deputy Chief of Staff for Prsnnl
Attn J Hiller
The Pentagon Rm 2C733
Washington DC 20301-0300

Dir of Chem & Nuc Ops DA DCSOPS
Attn Techl Lib
Washington DC 20301

SMC/CZA
2435 Vela Way Ste 1613
El Segundo CA 90245-5500

TECOM
Attn AMSTE-CL
Aberdeen Proving Ground MD 21005-5057

US Army ARDEC
Attn AMSTA-AR-TD M Fisette
Bldg 1
Picatinny Arsenal NJ 07806-5000

US Army Engrg Div
Attn HNDED FD
PO Box 1500
Huntsville AL 35807

US Army Info Sys Engrg Cmnd
Attn AMSEL-IE-TD F Jenia
FT Huachuca AZ 85613-5300

US Army Natick RDEC Acting Techl Dir
Attn SBCN-T P Brandler
Natick MA 01760-5002

US Army NGIC
Attn Rsrch & Data Branch
220 7th Stret NE
Charlottesville VA 22901-5396

US Army Nuc & Cheml Agency
7150 Heller Loop Ste 101
Springfield VA 22150-3198

US Army Simulation, Train, & Instrmntn Cmnd
Attn AMSTI-CG M Macedonia
Attn J Stahl
12350 Research Parkway
Orlando FL 32826-3726

US Army Soldier & Biol Chem Cmnd Dir of Rsrch & Techlgy Dirctrt
Attn SMCCR-RS I G Resnick
Aberdeen Proving Ground MD 21010-5423

US Army Strtgc Defns Cmnd
Attn CSSD H MPL Techl Lib
PO Box 1500
Huntsville AL 35807

Distribution (cont'd)

US Army Tank-Automtv Cmnd Rsrch, Dev, & Engrg Ctr
Attn AMSTA-TR J Chapin
Warren MI 48397-5000

US Army Train & Doctrine Cmnd
Battle Lab Integration & Techl Dirctrt
Attn ATCD-B
FT Monroe VA 23651-5850

US Military Academy
Mathematical Sci Ctr of Excellence
Attn MADN-MATH MAJ M Huber
Thayer Hall
West Point NY 10996-1786

Chief of Nav OPS Dept of the Navy
Attn OP 03EG
Washington DC 20350

Nav Surface Warfare Ctr
Attn Code B07 J Pennella
17320 Dahlgren Rd Bldg 1470 Rm 1101
Dahlgren VA 22448-5100

US Dept of Energy
Attn Techl Lib
Washington DC 20585

Central Intllgnc Agency
Dir DB Standard
Attn OSS/KPG/DHRT

1E61 OHB
Washington DC 20505

Hicks & Associates Inc
Attn G Singley III
1710 Goodrich Dr Ste 1300
McLean VA 22102

US Army Rsrch Ofc
Attn AMSRL-RO-D JCI Chang
Attn AMSRL-RO-EN W D Bach
Attn AMSRL-RO
PO Box 12211
Research Triangle Park NC 27709

US Army Rsrch Lab
Attn AMSRL-CI-AI-R Mail & Records Mgmt
Attn AMSRL-CI-AP Techl Pub (3 copies)
Attn AMSRL-CI-LL Techl Lib (3 copies)
Attn AMSRL-DD J M Miller
Attn AMSRL-IS-EE G Videen (10 copies)
Adelphi MD 20783-1197

REPORT DOCUMENTATION PAGE

Form Approved
OMB No. 0704-0188

1. AGENCY USE ONLY *(Leave blank)*	2. REPORT DATE	3. REPORT TYPE AND DATES COVERED
	September 2000	Final, FY99

4. TITLE AND SUBTITLE Light Scattering from Deformed Droplets and Droplets with Inclusions:
Volume II. Theoretical Results

5. FUNDING NUMBERS
DA PR: N/A
PE: 61102A

6. AUTHOR(S) Gorden Videen (ARL), Wenbo Sun, Qiang Fu (Dalhousie Univ., Canada), David Secker, Paul Kaye, Richard Greenaway, Edwin Hirst (Univ. of Hertfordshire, UK), David Bartley (National Instit. for Occupational Safety and Health)

7. PERFORMING ORGANIZATION NAME(S) AND ADDRESS(ES)
U.S. Army Research Laboratory
Attn: AMSRL-CI-EM email: gvideen@arl.army.mil
2800 Powder Mill Road
Adelphi, MD 20783-1197

8. PERFORMING ORGANIZATION REPORT NUMBER
ARL-TR-2228-II

9. SPONSORING/MONITORING AGENCY NAME(S) AND ADDRESS(ES)
U.S. Army Research Laboratory
2800 Powder Mill Road
Adelphi, MD 20783-1197

10. SPONSORING/MONITORING AGENCY REPORT NUMBER

11. SUPPLEMENTARY NOTES
ARL PR: 7FEJ70
AMS code: 61110253A11

12a. DISTRIBUTION/AVAILABILITY STATEMENT Approved for public release; distribution unlimited.

12b. DISTRIBUTION CODE

13. ABSTRACT *(Maximum 200 words)*

This is the second volume of a two-volume report dealing with experimental and theoretical results from the scattering of light by deformed liquid droplets and droplets with inclusions. With improved instrumentation and computer technologies available, researchers are able to employ two-dimensional angular optical scattering (TAOS) as a tool for analyzing such particle systems, and this could find application in industrial, occupational, and military aerosol measurements. In this report we present numerically calculated spatial light-scattering data from various droplet morphologies, which may be produced with a vibrating-orifice-type droplet generator. We describe characteristic features of the theoretical data and compare these to the experimental results given in volume I of this report.

14. SUBJECT TERMS Scattering, aerosols

15. NUMBER OF PAGES 27

16. PRICE CODE

17. SECURITY CLASSIFICATION OF REPORT	18. SECURITY CLASSIFICATION OF THIS PAGE	19. SECURITY CLASSIFICATION OF ABSTRACT	20. LIMITATION OF ABSTRACT
Unclassified	Unclassified	Unclassified	UL

NSN 7540-01-280-5500

Standard Form 298 (Rev. 2-89)
Prescribed by ANSI Std. Z39-18
298-102